

# Dynamics of entanglement in Two-Qubit Open System Interacting with a Squeezed Thermal Bath via Dissipative interaction

Subhashish Banerjee,<sup>1,2,\*</sup> V. Ravishankar,<sup>1,3,†</sup> and R. Srikanth<sup>4,1,‡</sup>

<sup>1</sup>*Raman Research Institute, Bangalore- 560080, India*

<sup>2</sup>*Chennai Mathematical Institute, Padur PO, Siruseri- 603103, India*

<sup>3</sup>*Indian Institute of Technology, Kanpur, India*

<sup>4</sup>*Poornaprajna Institute for Scientific Research, Bangalore- 560080, India*

We study the dynamics of entanglement in a two-qubit system interacting with a squeezed thermal bath via a dissipative system-reservoir interaction with the system and reservoir assumed to be in a separable initial state. The resulting entanglement is studied by making use of a recently introduced measure of mixed state entanglement via a probability density function which gives a statistical and geometrical characterization of entanglement by exploring the entanglement content in the various subspaces spanning the two-qubit Hilbert space. We also make an application of the two-qubit dissipative dynamics to a simplified model of quantum repeaters.

PACS numbers: 03.65.Yz, 03.67.Mn, 03.67.Bg, 03.67.Hk

## I. INTRODUCTION

Open quantum systems take into account the effect of the environment (reservoir or bath) on the dynamical evolution of the system of interest thereby providing a natural route for discussing damping and dephasing. One of the first testing grounds for open system ideas was in quantum optics [1]. Its application to other areas gained momentum from the works of Caldeira and Leggett [2], and Zurek [3], among others. The total Hamiltonian is  $H = H_S + H_R + H_{SR}$ , where  $S$  stands for the system,  $R$  for the reservoir and  $SR$  for the system-reservoir interaction. Depending upon the system-reservoir ( $S - R$ ) interaction, open systems can be broadly classified into two categories, viz., quantum non-demolition (QND) or dissipative. A particular type of quantum nondemolition (QND)  $S - R$  interaction is given by a class of energy-preserving measurements in which dephasing occurs without damping the system, i.e., where  $[H_S, H_{SR}] = 0$  while the dissipative systems correspond to the case where  $[H_S, H_{SR}] \neq 0$  resulting in decoherence along with dissipation [4].

A prototype of dissipative open quantum systems, having many applications, is the quantum Brownian motion of harmonic oscillators. This model was studied by Caldeira and Leggett [2] for the case where the system and its environment were initially separable. The above treatment of the quantum Brownian motion was generalized to the physically reasonable initial condition of a mixed state of the system and its environment by Hakim and Ambegaokar [5], Smith and Caldeira [6], Grabert, Schramm and Ingold [7], and for the case of a system in a Stern-Gerlach potential [8], and also for the quantum Brownian motion with nonlinear system-environment couplings [9], among others.

The interest in the relevance of open system ideas to quantum information has increased in recent times because of the impressive progress made on the experimental front in the manipulation of quantum states of matter towards quantum information processing and quantum communication. Myatt *et al.* [10] and Turchette *et al.* [11] have performed a series of experiments in which they induced decoherence and decay by coupling the atom (their system- $S$ ) to engineered reservoirs, in which the coupling to, and the state of, the environment are controllable.

Quantum entanglement is the inherent property of a system to exhibit correlations, the physical basis being the non-local nature of quantum mechanics [12], and hence is a property that is exclusively quantum in nature. Entanglement plays a central role in quantum information theory [13] as in interesting non-classical applications such as quantum computation [14] and quantum error correction [15]. A number of methods have been proposed for creating entanglement involving trapped atoms [16, 17, 18].

An important issue is to study how quantum entanglement is affected by noise, which can be thought of as a manifestation of an open system effect [19]. In [20] entanglement of a two-mode squeezed state in a phase-sensitive Gaussian environment was studied and the criteria for the necessary and sufficient condition for separability of Gaussian continuous-variable states [21] was employed as a measure of entanglement. In [22] the entanglement between

---

\*Electronic address: subhashish@cmi.ac.in

†Electronic address: vravi@iitk.ac.in

‡Electronic address: srik@rri.res.in

charge qubits induced by a common dissipative environment was analyzed using concurrence as the measure. Some recent experimental investigations on the influence of decoherence on the dynamics of entanglement have been made in [23, 24]. In a related work [25], this issue was taken up with the noise coming from the effect of the environment modelled by a QND  $S - R$  interaction. Here we complement this program by studying the effect of noise, modelled by a dissipative  $S - R$  interaction with the reservoir in an initial squeezed-thermal state [4, 26], on the entanglement evolution between two spatially separated (and initially uncorrelated) qubits, brought out by interaction with the bath. This would be of relevance to evaluate the performance of two-qubit gates in practical quantum information processing systems.

Since we are dealing here with a two qubit system which very rapidly evolves into a mixed state, a study of entanglement would necessarily involve a measure of entanglement for mixed states. Entanglement of a bipartite system in a pure state is unambiguous and well defined. However, mixed state entanglement (MSE) is not so well defined. Thus, although a number of criteria such as entanglement of formation [27, 28, 29] and separability [30] exist, there is a realization [27] that a single quantity is inadequate to describe MSE. This was the principal motivation for the development of a new prescription of MSE [31] in which it is characterized not as a function, but as a probability density function (PDF). The known prescriptions such as concurrence and negativity emerge as particular parameters that characterize the probability density. We will principally make use of this measure in our study of entanglement in the two-qubit system.

The plan of the paper is as follows. In Section II, we recapitulate for consistency, the recently developed entanglement measure of MSE [31]. In Section III, the master equation describing the dynamical evolution of the two-qubit system interacting with a squeezed thermal bath, via a dissipative  $S - R$  interaction, is given which is then used in Section IV, to study in detail the dynamics of the system interacting with a vacuum bath with zero bath squeezing in Section IV(A) and with a general squeezed thermal bath in Section IV(B). Section V deals with the entanglement analysis of the two-qubit open system using the PDF as a measure of entanglement. We compare it with the usual measure of MSE, concurrence. We dwell on the scenarios where the two qubits effectively interact via localized  $S - R$  interactions, called the independent decoherence model, as also when they interact collectively with the bath, called the collective decoherence model. In Section VI, we make a brief application of the model to practical quantum communication, in the form of a quantum repeater [32, 33]. In Section VII, we make our conclusions.

## II. CHARACTERIZATION OF MIXED STATE ENTANGLEMENT THROUGH A PROBABILITY DENSITY FUNCTION

Here we briefly recapitulate the characterization of mixed state entanglement (MSE) through a PDF as developed in [31]. As pointed out in the Introduction, the above criterion was evolved from the motivation that for the characterization of MSE, a single parameter is inadequate. The basic idea is to express the PDF of entanglement of a given system density matrix (in this case, a two-qubit) in terms of a weighted sum over the PDF's of projection operators spanning the full Hilbert space of the system density matrix. The PDF of a system in a state which is a projection operator  $\rho = \frac{1}{M}\Pi_M$  of rank  $M$  is defined as:

$$\mathcal{P}_{\Pi_M}(\mathcal{E}) = \frac{\int d\mathcal{H}_{\Pi_M} \delta(\mathcal{E}_\psi - \mathcal{E})}{\int d\mathcal{H}_{\Pi_M}}, \quad (1)$$

where  $\int d\mathcal{H}_{\Pi_M}$  is the volume measure for  $\mathcal{H}_{\Pi_M}$ , which is the subspace spanned by  $\Pi_M$ . The volume measure is determined by the invariant Haar measure associated with the group of automorphisms of  $\int d\mathcal{H}_{\Pi_M}$ , modulo the stabilizer group of the reference state generating  $\mathcal{H}_{\Pi_M}$ . Thus for a one dimensional projection operator, representing a pure state, the group of automorphisms consists of only the identity element and the PDF is simply given by the Dirac delta. Indeed, if  $\rho = \Pi_1 \equiv |\psi\rangle\langle\psi|$ , the PDF has the form  $\mathcal{P}_\rho(\mathcal{E}) = \delta(\mathcal{E} - \mathcal{E}_\psi)$  thereby resulting in the description of pure state entanglement, as expected, by a single number. The entanglement density of a system in a general mixed state  $\rho$  is given by resolving it in terms of nested projection operators with appropriate weights as

$$\begin{aligned} \rho &= (\lambda_1 - \lambda_2)\Pi_1 + (\lambda_2 - \lambda_3)\Pi_2 + \dots + (\lambda_{N-1} - \lambda_N)\Pi_{N-1} + \lambda_N\Pi_N \\ &\equiv \sum_{M=1}^N \Lambda_M \Pi_M, \end{aligned} \quad (2)$$

where the projections are  $\Pi_M = \sum_{j=1}^M |\psi_j\rangle\langle\psi_j|$ , with  $M = 1, 2, \dots, N$  and the eigenvalues  $\lambda_1 \geq \lambda_2 \geq \dots$ , i.e., the eigenvalues are arranged in a non-increasing fashion. Thus the PDF for the entanglement of  $\rho$  is given by

$$\mathcal{P}_\rho(\mathcal{E}) = \sum_{M=1}^N \omega_M \mathcal{P}_{\Pi_M}(\mathcal{E}), \quad (3)$$

where the weights of the respective projections  $\mathcal{P}_{\Pi_M}(\mathcal{E})$  are given by  $\omega_M = \Lambda_M/\lambda_1$ . For a two qubit system, the density matrix would be represented as a nested sum over four projection operators,  $\Pi_1, \Pi_2, \Pi_3, \Pi_4$  corresponding to one, two, three and four dimensional projections, respectively, with  $\Pi_1$  corresponding to a pure state and  $\Pi_4$  corresponding to a uniformly mixed state, is a multiple of the identity operator. The most interesting structure is present in  $\Pi_2$ , the two-dimensional projection, which is characterized by three parameters, viz.  $\mathcal{E}_{cusp}$ , the entanglement at which the PDF diverges,  $\mathcal{E}_{max}$ , the maximum entanglement allowed and  $\mathcal{P}_2(\mathcal{E}_{max})$ , the PDF corresponding to  $\mathcal{E}_{max}$ . The three dimensional projection  $\Pi_3$  is characterized by the parameter  $\mathcal{E}_1$ , which parametrizes a discontinuity in the entanglement density function curve. By virtue of the convexity of the sum over the nested projections (2), it can be seen that the concurrence of any state  $\rho$  is given by the inequality  $C_\rho \leq (\lambda_1 - \lambda_2)\mathcal{C}_{\Pi_1} + (\lambda_2 - \lambda_3)\mathcal{C}_{\Pi_2}$ . Thus while the concurrence for a three and four dimensional projection is identically zero, through the PDF one is able to make a statement about the entanglement content of these spaces. The fact that the PDF (3) enables us to study entanglement of a physical state by exploiting the richness inherent in the subspaces spanned by the system Hilbert space makes it an attractive statistical and geometric characterization of entanglement, of which an explicit illustration is made in Section V.

### III. TWO-QUBIT DISSIPATIVE INTERACTION WITH A SQUEEZED THERMAL BATH

We consider the Hamiltonian, describing the dissipative interaction of  $N$  qubits (two-level atomic system) with the bath (modelled as a 3-D electromagnetic field (EMF)) via the dipole interaction as [34]

$$\begin{aligned} H &= H_S + H_R + H_{SR} \\ &= \sum_{n=1}^N \hbar\omega_n S_n^z + \sum_{\vec{k}s} \hbar\omega_k (b_{\vec{k}s}^\dagger b_{\vec{k}s} + 1/2) - i\hbar \sum_{\vec{k}s} \sum_{n=1}^N [\vec{\mu}_n \cdot \vec{g}_{\vec{k}s}(\vec{r}_n) (S_n^+ + S_n^-) b_{\vec{k}s} - h.c.]. \end{aligned} \quad (4)$$

Here  $\vec{\mu}_n$  are the transition dipole moments, dependent on the different atomic positions  $\vec{r}_n$  and

$$S_n^+ = |e_n\rangle\langle g_n|, \quad S_n^- = |g_n\rangle\langle e_n|, \quad (5)$$

are the dipole raising and lowering operators satisfying the usual commutation relations and

$$S_n^z = \frac{1}{2}(|e_n\rangle\langle e_n| - |g_n\rangle\langle g_n|), \quad (6)$$

is the energy operator of the  $n$ th atom, while  $b_{\vec{k}s}^\dagger, b_{\vec{k}s}$  are the creation and annihilation operators of the field mode (bath)  $\vec{k}s$  with the wave vector  $\vec{k}$ , frequency  $\omega_k$  and polarization index  $s = 1, 2$  with the system-reservoir (S-R) coupling constant

$$\vec{g}_{\vec{k}s}(\vec{r}_n) = \left(\frac{\omega_k}{2\epsilon\hbar V}\right)^{1/2} \vec{e}_{\vec{k}s} e^{i\vec{k}\cdot\vec{r}_n}. \quad (7)$$

Here  $V$  is the normalization volume and  $\vec{e}_{\vec{k}s}$  is the unit polarization vector of the field. It can be seen from Eq. (7) that the S-R coupling constant is dependent on the atomic position  $r_n$ . This leads to a number of interesting dynamical aspects, as seen below. From now we will concentrate on the case of two qubits. Assuming separable initial conditions, and taking a trace over the bath the reduced density matrix of the qubit system in the interaction picture and in the usual Born-Markov, rotating wave approximation (RWA) is obtained as [34]

$$\begin{aligned} \frac{d\rho}{dt} &= -\frac{i}{\hbar}[H_{\bar{S}}, \rho] - \frac{1}{2} \sum_{i,j=1}^2 \Gamma_{ij} [1 + \tilde{N}] (\rho S_i^+ S_j^- + S_i^+ S_j^- \rho - 2S_j^- \rho S_i^+) \\ &\quad - \frac{1}{2} \sum_{i,j=1}^2 \Gamma_{ij} \tilde{N} (\rho S_i^- S_j^+ + S_i^- S_j^+ \rho - 2S_j^+ \rho S_i^-) + \frac{1}{2} \sum_{i,j=1}^2 \Gamma_{ij} \tilde{M} (\rho S_i^+ S_j^+ + S_i^+ S_j^+ \rho - 2S_j^+ \rho S_i^+) \\ &\quad + \frac{1}{2} \sum_{i,j=1}^2 \Gamma_{ij} \tilde{M}^* (\rho S_i^- S_j^- + S_i^- S_j^- \rho - 2S_j^- \rho S_i^-). \end{aligned} \quad (8)$$

In Eq. (8)

$$\tilde{N} = N_{\text{th}}(\cosh^2(r) + \sinh^2(r)) + \sinh^2(r), \quad (9)$$

$$\tilde{M} = -\frac{1}{2} \sinh(2r) e^{i\Phi} (2N_{\text{th}} + 1) \equiv R e^{i\Phi(\omega_0)}, \quad (10)$$

with

$$\omega_0 = \frac{\omega_1 + \omega_2}{2}, \quad (11)$$

and

$$N_{\text{th}} = \frac{1}{e^{\frac{\hbar\omega}{k_B T}} - 1}. \quad (12)$$

Here  $N_{\text{th}}$  is the Planck distribution giving the number of thermal photons at the frequency  $\omega$  and  $r, \Phi$  are squeezing parameters. The analogous case of a thermal bath without squeezing can be obtained from the above expressions by setting these squeezing parameters to zero, while setting the temperature ( $T$ ) to zero one recovers the case of the vacuum bath. Eq. (8), for a single qubit case, can be solved using the Bloch vector formalism (cf. [19], [35]) and also in the superoperator formalism [36]. Here the assumption of perfect matching of the squeezed modes to the modes of the EMF is made along with, the squeezing bandwidth being much larger than the atomic linewidths. Also, the squeezing carrier frequency is taken to be tuned in resonance with the atomic frequencies.

In Eq. (8),

$$H_{\bar{S}} = \hbar \sum_{n=1}^2 \omega_n S_n^z + \hbar \sum_{\substack{i,j \\ (i \neq j)}}^2 \Omega_{ij} S_i^+ S_j^-, \quad (13)$$

where

$$\begin{aligned} \Omega_{ij} &= \frac{3}{4} \sqrt{\Gamma_i \Gamma_j} \left[ -[1 - (\hat{\mu} \cdot \hat{r}_{ij})^2] \frac{\cos(k_0 r_{ij})}{k_0 r_{ij}} + [1 - 3(\hat{\mu} \cdot \hat{r}_{ij})^2] \right. \\ &\quad \left. \times \left[ \frac{\sin(k_0 r_{ij})}{(k_0 r_{ij})^2} + \frac{\cos(k_0 r_{ij})}{(k_0 r_{ij})^3} \right] \right]. \end{aligned} \quad (14)$$

Here  $\hat{\mu} = \hat{\mu}_1 = \hat{\mu}_2$  and  $\hat{r}_{ij}$  are unit vectors along the atomic transition dipole moments and  $\vec{r}_{ij} = \vec{r}_i - \vec{r}_j$ , respectively. Also  $k_0 = \omega_0/c$ , with  $\omega_0$  being as in Eq. (11),  $r_{ij} = |\vec{r}_{ij}|$ . The wavevector  $k_0 = 2\pi/\lambda_0$ ,  $\lambda_0$  being the resonant wavelength, occurring in the term  $k_0 r_{ij}$  sets up a length scale into the problem depending upon the ratio  $r_{ij}/\lambda_0$ . This is thus the ratio between the interatomic distance and the resonant wavelength, allowing for a discussion of the dynamics in two regimes: (A). independent decoherence where  $k_0 r_{ij} \sim \frac{r_{ij}}{\lambda_0} \geq 1$  and (B). collective decoherence where  $k_0 r_{ij} \sim \frac{r_{ij}}{\lambda_0} \rightarrow 0$ . The case (B) of collective decoherence would arise when the qubits are close enough for them to feel the bath collectively or when the bath has a long correlation length (set by the resonant wavelength  $\lambda_0$ ) in comparison to the interqubit separation  $r_{ij}$ .  $\Omega_{ij}$  (14) is a collective coherent effect due to the multi-qubit interaction and is mediated via the bath through the terms

$$\Gamma_i = \frac{\omega_i^3 \mu_i^2}{3\pi\epsilon\hbar c^3}. \quad (15)$$

The term  $\Gamma_i$  is present even in the case of single-qubit dissipative system bath interaction [35, 36] and is the spontaneous emission rate, while

$$\Gamma_{ij} = \Gamma_{ji} = \sqrt{\Gamma_i \Gamma_j} F(k_0 r_{ij}), \quad (16)$$

where  $i \neq j$  with

$$\begin{aligned} F(k_0 r_{ij}) &= \frac{3}{2} \left[ [1 - (\hat{\mu} \cdot \hat{r}_{ij})^2] \frac{\sin(k_0 r_{ij})}{k_0 r_{ij}} + [1 - 3(\hat{\mu} \cdot \hat{r}_{ij})^2] \right. \\ &\quad \left. \times \left[ \frac{\cos(k_0 r_{ij})}{(k_0 r_{ij})^2} - \frac{\sin(k_0 r_{ij})}{(k_0 r_{ij})^3} \right] \right]. \end{aligned} \quad (17)$$

$\Gamma_{ij}$  (16) is the collective incoherent effect due to the dissipative multi-qubit interaction with the bath. For the case of identical qubits, as considered here,  $\Omega_{12} = \Omega_{21}$ ,  $\Gamma_{12} = \Gamma_{21}$  and  $\Gamma_1 = \Gamma_2 = \Gamma$ .

#### IV. DYNAMICS OF THE TWO-QUBIT DISSIPATIVE INTERACTION WITH A VACUUM AND SQUEEZED THERMAL BATH

Here we present the solutions of the density matrix equation (8) for the case of a two-qubit system interacting with a (A). vacuum bath and (B). squeezed thermal bath. These results will be of use in the investigation of the dynamics of entanglement subsequently.

##### A. Vacuum bath

Here we proceed as in [34] and obtain the reduced density matrix from Eq. (8), setting  $T$  and bath squeezing to zero, and by going over to the dressed state basis, of the collective two-qubit dynamics, obtained from the Hamiltonian  $H_{\bar{S}}$  (13) as

$$\begin{aligned} |g\rangle &= |g_1\rangle|g_2\rangle, \\ |s\rangle &= \frac{1}{\sqrt{2}}(|e_1\rangle|g_2\rangle + |g_1\rangle|e_2\rangle), \\ |a\rangle &= \frac{1}{\sqrt{2}}(|e_1\rangle|g_2\rangle - |g_1\rangle|e_2\rangle), \\ |e\rangle &= |e_1\rangle|e_2\rangle, \end{aligned} \quad (18)$$

with the corresponding eigenvalues being  $E_g = -\hbar\omega_0$ ,  $E_s = \hbar\Omega_{12}$ ,  $E_a = -\hbar\Omega_{12}$  and  $E_e = \hbar\omega_0$ . The reduced density matrix in the dressed state basis (18) can be obtained from Eq. (8) as

$$\frac{d\rho}{dt} = -\frac{i}{\hbar}[H_{as}, \rho] + \left(\frac{d\rho}{dt}\right)_s + \left(\frac{d\rho}{dt}\right)_a, \quad (19)$$

where

$$H_{as} = \hbar[\omega_0(|e\rangle\langle e| - |g\rangle\langle g|) + \Omega_{12}(|s\rangle\langle s| - |a\rangle\langle a|)], \quad (20)$$

$$\begin{aligned} \left(\frac{d\rho}{dt}\right)_s &= -\frac{1}{2}(\Gamma + \Gamma_{12})[ (|e\rangle\langle e| + |s\rangle\langle s|)\rho + \rho(|e\rangle\langle e| + |s\rangle\langle s|) \\ &\quad - 2(|s\rangle\langle e| + |g\rangle\langle s|)\rho(|e\rangle\langle s| + |s\rangle\langle g|)], \end{aligned} \quad (21)$$

and

$$\begin{aligned} \left(\frac{d\rho}{dt}\right)_a &= -\frac{1}{2}(\Gamma - \Gamma_{12})[ (|e\rangle\langle e| + |a\rangle\langle a|)\rho + \rho(|e\rangle\langle e| + |a\rangle\langle a|) \\ &\quad - 2(|a\rangle\langle e| - |g\rangle\langle a|)\rho(|e\rangle\langle a| - |a\rangle\langle g|)]. \end{aligned} \quad (22)$$

From the dressed state basis (18), it can be seen that the two-qubit problem can be thought of as an equivalent four-level system. For the case where  $r_{ij}/\lambda_0 \rightarrow 0$ , i.e., when the interatomic separation is much smaller than the resonant wavelength, constituting the Dicke model [37],  $(d\rho/dt)_a = 0$  and the problem reduces to an effective three-level system. The Eq. (19) can be solved to yield the various density matrix elements as follows:

$$\rho_{ee}(t) = e^{-2\Gamma t} \rho_{ee}(0), \quad (23)$$

$$\rho_{ss}(t) = e^{-(\Gamma+\Gamma_{12})t} \rho_{ss}(0) + \frac{(\Gamma + \Gamma_{12})}{(\Gamma - \Gamma_{12})} (1 - e^{-(\Gamma-\Gamma_{12})t}) e^{-(\Gamma+\Gamma_{12})t} \rho_{ee}(0), \quad (24)$$

$$\rho_{aa}(t) = e^{-(\Gamma-\Gamma_{12})t} \rho_{aa}(0) + \frac{(\Gamma - \Gamma_{12})}{(\Gamma + \Gamma_{12})} (1 - e^{-(\Gamma+\Gamma_{12})t}) e^{-(\Gamma-\Gamma_{12})t} \rho_{ee}(0), \quad (25)$$

$$\begin{aligned} \rho_{gg}(t) &= \rho_{gg}(0) + (1 - e^{-(\Gamma+\Gamma_{12})t}) \rho_{ss}(0) + (1 - e^{-(\Gamma-\Gamma_{12})t}) \rho_{aa}(0) \\ &\quad + \left[ \frac{(\Gamma + \Gamma_{12})}{2\Gamma} \left\{ 1 - \frac{2}{(\Gamma - \Gamma_{12})} \left[ \frac{(\Gamma + \Gamma_{12})}{2} (1 - e^{-(\Gamma-\Gamma_{12})t}) + \frac{(\Gamma - \Gamma_{12})}{2} \right] e^{-(\Gamma+\Gamma_{12})t} \right\} \right. \\ &\quad \left. + \frac{(\Gamma - \Gamma_{12})}{(\Gamma + \Gamma_{12})} \left\{ (1 - e^{-(\Gamma-\Gamma_{12})t}) - \frac{(\Gamma - \Gamma_{12})}{2\Gamma} (1 - e^{-2\Gamma t}) \right\} \right] \rho_{ee}(0). \end{aligned} \quad (26)$$

The Eqs. (23) to (26) give the dynamics of the population of the two-qubit system interacting with a vacuum bath and  $\rho_{ee}(t) + \rho_{ss}(t) + \rho_{aa}(t) + \rho_{gg}(t) = \rho_{ee}(0) + \rho_{ss}(0) + \rho_{aa}(0) + \rho_{gg}(0)$ . The off-diagonal terms of the density matrix are:

$$\begin{aligned}\rho_{es}(t) &= e^{-i(\omega_0 - \Omega_{12})t} e^{-\frac{1}{2}(3\Gamma + \Gamma_{12})t} \rho_{es}(0), \\ \rho_{se}(t) &= \rho_{es}^*(t),\end{aligned}\tag{27}$$

$$\begin{aligned}\rho_{eg}(t) &= e^{-i2\omega_0 t} e^{-\Gamma t} \rho_{eg}(0), \\ \rho_{ge}(t) &= \rho_{eg}^*(t),\end{aligned}\tag{28}$$

$$\begin{aligned}\rho_{ea}(t) &= e^{-i(\omega_0 + \Omega_{12})t} e^{-\frac{1}{2}(3\Gamma - \Gamma_{12})t} \rho_{ea}(0), \\ \rho_{ae}(t) &= \rho_{ea}^*(t),\end{aligned}\tag{29}$$

$$\begin{aligned}\rho_{sa}(t) &= e^{-i2\Omega_{12}t} e^{-\Gamma t} \rho_{sa}(0), \\ \rho_{as}(t) &= \rho_{sa}^*(t),\end{aligned}\tag{30}$$

$$\begin{aligned}\rho_{ag}(t) &= e^{-i(\omega_0 - \Omega_{12})t} e^{-\frac{1}{2}(\Gamma - \Gamma_{12})t} \rho_{ag}(0) - \frac{(\Gamma - \Gamma_{12})}{(\Gamma^2 + 4\Omega_{12}^2)} e^{-i(\omega_0 - \Omega_{12})t} \\ &\quad \times e^{-\frac{1}{2}(\Gamma - \Gamma_{12})t} [2\Omega_{12} e^{-\Gamma t} \sin(2\Omega_{12}t) + \Gamma(1 - e^{-\Gamma t} \cos(2\Omega_{12}t))] \rho_{ea}(0) \\ &\quad + i \frac{(\Gamma - \Gamma_{12})}{(\Gamma^2 + 4\Omega_{12}^2)} e^{-i(\omega_0 - \Omega_{12})t} e^{-\frac{1}{2}(\Gamma - \Gamma_{12})t} [2\Omega_{12}(1 - e^{-\Gamma t} \cos(2\Omega_{12}t)) \\ &\quad - \Gamma e^{-\Gamma t} \sin(2\Omega_{12}t)] \rho_{ea}(0), \\ \rho_{ga}(t) &= \rho_{ag}^*(t),\end{aligned}\tag{31}$$

$$\begin{aligned}\rho_{sg}(t) &= e^{-i(\omega_0 + \Omega_{12})t} e^{-\frac{1}{2}(\Gamma + \Gamma_{12})t} \rho_{sg}(0) + \frac{(\Gamma + \Gamma_{12})}{(\Gamma^2 + 4\Omega_{12}^2)} e^{-i(\omega_0 + \Omega_{12})t} \\ &\quad \times e^{-\frac{1}{2}(\Gamma + \Gamma_{12})t} [2\Omega_{12} e^{-\Gamma t} \sin(2\Omega_{12}t) + \Gamma(1 - e^{-\Gamma t} \cos(2\Omega_{12}t))] \rho_{es}(0) \\ &\quad + i \frac{(\Gamma + \Gamma_{12})}{(\Gamma^2 + 4\Omega_{12}^2)} e^{-i(\omega_0 + \Omega_{12})t} e^{-\frac{1}{2}(\Gamma + \Gamma_{12})t} [2\Omega_{12}(1 - e^{-\Gamma t} \cos(2\Omega_{12}t)) \\ &\quad - \Gamma e^{-\Gamma t} \sin(2\Omega_{12}t)] \rho_{es}(0), \\ \rho_{gs}(t) &= \rho_{sg}^*(t).\end{aligned}\tag{32}$$

The sixteen density matrix elements given by Eqs. (23) to (32) completely solve the master equation (19) describing the dynamics of the two-qubit system interacting with the vacuum bath. For the case of the Dicke model, where  $r_{ij}/\lambda_0 \rightarrow 0$ , i.e., when the interatomic separation is much smaller than the resonant wavelength,  $(d\rho/dt)_a = 0$  and the solution of the effective three-level system can be extracted out of the above equations. The conditions under which the Dicke model is obtained is analogous to the case of collective decoherence for the case of two-qubit interaction with a bath via a quantum nondemolition interaction (QND) [25]. There it was found that for the case of interaction with a thermal (and also a vacuum) bath, the subspace spanned by  $\{|e_1, g_2\rangle, |g_1, e_2\rangle\}$  is a decoherence-free subspace, implying that the matrix elements  $\rho_{e_1, g_2; e_1, g_2}, \rho_{g_1, e_2; g_1, e_2}, \rho_{e_1, g_2; g_1, e_2}$  and  $\rho_{g_1, e_2; e_1, g_2}$  remain invariant inspite of the system's interaction with a bath. However, from Eqs. (23)–(32) it is clear that none of the matrix elements is invariant as a function of time, reflecting the greater complexity of the dissipative interaction.

## B. Squeezed thermal bath

Here we consider the two-qubit dynamics resulting from an interaction with a squeezed thermal bath, i.e., make use of Eq. (8). The equations of the reduced density matrix (8) taken in the two-qubit dressed state basis (18) are not all mutually coupled, but divide into four irreducible blocks A, B, C, D, thereby reducing the task from an evaluation of fifteen coupled linear differential equations to that of a maximum of four coupled equations. Thus we have:

Block A:

$$\begin{aligned}
\dot{\rho}_{ee}(t) &= -2\Gamma(\tilde{N} + 1)\rho_{ee}(t) + \tilde{N}\left\{(\Gamma + \Gamma_{12})\rho_{ss}(t) + (\Gamma - \Gamma_{12})\rho_{aa}(t)\right\} + \Gamma_{12}|\tilde{M}|\rho_u(t), \\
\dot{\rho}_{ss}(t) &= -(\Gamma + \Gamma_{12})\left\{-\tilde{N} + (1 + 3\tilde{N})\rho_{ss}(t) - \rho_{ee}(t) + \tilde{N}\rho_{aa}(t) + |\tilde{M}|\rho_u(t)\right\}, \\
\dot{\rho}_{aa}(t) &= (\Gamma - \Gamma_{12})\left\{\tilde{N} - (1 + 3\tilde{N})\rho_{aa}(t) + \rho_{ee}(t) - \tilde{N}\rho_{ss}(t) + |\tilde{M}|\rho_u(t)\right\}, \\
\dot{\rho}_u(t) &= 2|\tilde{M}|\Gamma_{12} - 4\omega_0|\rho_{ge}|\sin(\Phi + \chi) - (2\tilde{N} + 1)\Gamma\rho_u - 2|\tilde{M}|\left\{(\Gamma + 2\Gamma_{12})\rho_{ss}(t) - (\Gamma - 2\Gamma_{12})\rho_{aa}(t)\right\}. \quad (33)
\end{aligned}$$

Here

$$\rho_u(t) = e^{i\Phi}\rho_{ge}(t) + h.c., \quad (34)$$

$\rho_{ge} = |\rho_{ge}|e^{i\chi}$  and  $\Phi$  is as in Eq. (10). Also  $\rho_{gg}(t) = 1 - \rho_{aa}(t) - \rho_{ss}(t) - \rho_{ee}(t)$ . The Eqs. (33) give the dynamics of the population of the two-qubit system interacting with a squeezed thermal bath while the off-diagonal terms, given by the Blocks B, C and D are:

Block B:

$$\begin{aligned}
\dot{\rho}_{es}(t) &= -i(\omega_0 - \Omega_{12})\rho_{es}(t) - \frac{1}{2}\left\{(3\Gamma + \Gamma_{12}) + 2\tilde{N}(2\Gamma + \Gamma_{12})\right\}\rho_{es}(t) + \tilde{N}(\Gamma + \Gamma_{12})\rho_{sg}(t) \\
&\quad + \tilde{M}\Gamma_{12}\rho_{gs}(t) - \tilde{M}(\Gamma + \Gamma_{12})\rho_{se}(t), \\
\dot{\rho}_{se}(t) &= \dot{\rho}_{es}^*(t), \\
\dot{\rho}_{gs}(t) &= -i(\omega_0 - \Omega_{12})\rho_{gs}(t) - \frac{1}{2}\left\{(\Gamma + \Gamma_{12}) + 2\tilde{N}(2\Gamma + \Gamma_{12})\right\}\rho_{gs}(t) + (1 + \tilde{N})(\Gamma + \Gamma_{12})\rho_{se}(t) \\
&\quad + \tilde{M}^*\Gamma_{12}\rho_{es}(t) - \tilde{M}^*(\Gamma + \Gamma_{12})\rho_{sg}(t), \\
\dot{\rho}_{sg}(t) &= \dot{\rho}_{gs}^*(t). \quad (35)
\end{aligned}$$

Block C:

$$\begin{aligned}
\dot{\rho}_{as}(t) &= i2\Omega_{12}\rho_{as}(t) - \Gamma(1 + 2\tilde{N})\rho_{as}(t), \\
\dot{\rho}_{sa}(t) &= \dot{\rho}_{as}^*(t). \quad (36)
\end{aligned}$$

Block D:

$$\begin{aligned}
\dot{\rho}_{ea}(t) &= -i(\omega_0 + \Omega_{12})\rho_{ea}(t) - \frac{1}{2}\left\{(3\Gamma - \Gamma_{12}) + 2\tilde{N}(2\Gamma - \Gamma_{12})\right\}\rho_{ea}(t) - \tilde{N}(\Gamma - \Gamma_{12})\rho_{ag}(t) \\
&\quad + \tilde{M}\Gamma_{12}\rho_{ga}(t) - \tilde{M}(\Gamma - \Gamma_{12})\rho_{ae}(t), \\
\dot{\rho}_{ae}(t) &= \dot{\rho}_{ea}^*(t), \\
\dot{\rho}_{ga}(t) &= i(\omega_0 - \Omega_{12})\rho_{ga}(t) - \frac{1}{2}\left\{(\Gamma - \Gamma_{12}) + 2\tilde{N}(2\Gamma - \Gamma_{12})\right\}\rho_{ga}(t) - (1 + \tilde{N})(\Gamma - \Gamma_{12})\rho_{ae}(t) \\
&\quad + \tilde{M}^*\Gamma_{12}\rho_{ea}(t) - \tilde{M}^*(\Gamma - \Gamma_{12})\rho_{ag}(t), \\
\dot{\rho}_{ag}(t) &= \dot{\rho}_{ga}^*(t). \quad (37)
\end{aligned}$$

The Eqs. (36) can be trivially solved to yield

$$\begin{aligned}
\rho_{as}(t) &= e^{[i2\Omega_{12} - \Gamma(1 + 2\tilde{N})]t}\rho_{as}(0) \\
\rho_{sa}(t) &= \rho_{as}^*(t), \quad (38)
\end{aligned}$$

while the blocks A, B and D consist of four linear coupled differential equations which can be written in matrix form as:

$$\dot{P}(t) = -QP(t) + W, \quad (39)$$

where  $Q$  is a time-independent  $4 \times 4$  matrix and  $P(t)$ ,  $W$  are  $4 \times 1$  column vectors. The Eq. (39) has the general solution

$$P(t) = (Ve^{-Dt}V^{-1})P(0) + VD^{-1}(1 - e^{-Dt})V^{-1}W. \quad (40)$$



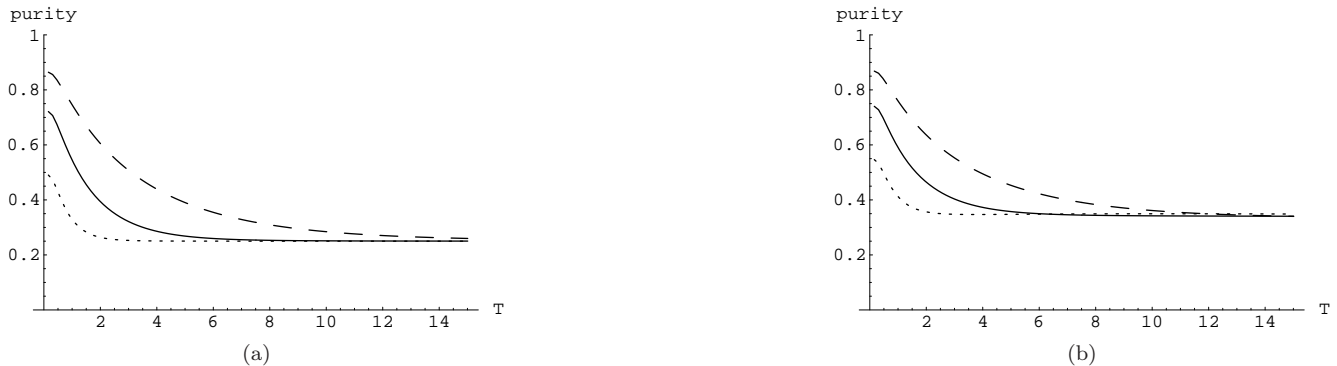


FIG. 1: Purity as a function of temperature  $T$  (in units where  $\hbar \equiv k_B = 1$ ) for (a) the independent decoherence model, where  $r_{ij}/\lambda_0$  (14) is  $\geq 1$  and (b) the collective decoherence model, where  $r_{ij}/\lambda_0$  (14) is  $\approx 0$ . Here with  $r_{12}$  is the inter-qubit distance. The large-dashed, bold and dotted curves correspond to evolution time  $t = 1.0$  and bath squeezing parameter (9, 10)  $r = -0.5$ , 1.0 and 1.5, respectively. Here and in all the subsequent figures, the squeezing parameter  $\Phi$  (10) is set equal to zero. Also  $\omega_0$  (11) and the bath parameter  $\Gamma$  (15), are set equal to 1.0 and 0.05, respectively. All the inter-qubit distances are defined on the scale of the resonant wavelength coming from the wavevector  $k$  (7) as a result of the position dependent couplings of the qubits with the bath. In figure (a) related to the independent decoherence model,  $kr_{12}$  is set equal to 1.5 while in figure (b) related to the collective decoherence model,  $kr_{12}$  is set equal to 0.08.

Here  $V$  is the vector composed of the eigenvectors of the matrix  $Q$ , while  $D$  is composed of its eigenvalues. We solve Eq. (40) by numerically obtaining the eigenvalues and eigenvectors of the matrix  $Q$  for the Blocks A, B, C, and D.

Figures (1 (a)), (b) depict the behavior of purity, defined here as  $\text{Tr}(\rho^2(t))$  for  $\rho(t)$  as obtained in this subsection for the independent ( $k_0.r_{ij} \neq 0$ ) and collective ( $k_0.r_{ij} \rightarrow 0$ ) decoherence model, respectively, as a function of temperature  $T$  for an evolution time  $t$  and bath squeezing  $r$  (9, 10). In all the figures in this article, we consider the initial state of one qubit in the excited state  $|e_1\rangle$  and the other in the ground state  $|g_2\rangle$ , i.e.,  $|e_1\rangle|g_2\rangle$  and  $\hat{\mu}.\hat{r}_{ij}$  (17) is equal to zero. It can be seen that with the increase in temperature, as also evolution time  $t$  and bath squeezing  $r$ , the system becomes more mixed and hence loses its purity.

## V. ENTANGLEMENT ANALYSIS

In this section, we will study the development of entanglement in the two qubit system, both for the independent as well as the collective decoherence model interacting with a squeezed thermal bath. A well known measure of MSE is the concurrence [28] defined as

$$\mathcal{C} = \max(0, \sqrt{\lambda_1} - \sqrt{\lambda_2} - \sqrt{\lambda_3} - \sqrt{\lambda_4}), \quad (41)$$

where  $\lambda_i$  are the eigenvalues of the matrix

$$R = \rho\tilde{\rho}, \quad (42)$$

with  $\tilde{\rho} = \sigma_y \otimes \sigma_y \rho^* \sigma_y \otimes \sigma_y$  and  $\sigma_y$  is the usual Pauli matrix.  $\mathcal{C}$  is zero for unentangled states and one for maximally entangled states. Since the reduced dynamics of the two-qubit system was obtained in the dressed state basis (18), which contains entangled states, in order to remove spurious entanglement coming from the basis, for the entanglement analysis we rotate the density operator back to a separable basis by means of a Hadamard transformation acting in the subspace spanned by  $\{|a\rangle, |s\rangle\}$ , i.e., the tensor sum of a Hadamard in this subspace and an identity operation in the subspace spanned by  $\{|e\rangle, |g\rangle\}$ , i.e.,  $H_{(as)} \oplus I_{(eg)}$ .

Here we study concurrence for the two-qubit system interacting with a squeezed vacuum bath. In figure (2) concurrence is plotted for the initial state  $|e_1\rangle|g_2\rangle$  for both the independent as well as collective dynamics. Figure (3) depicts the behavior of concurrence for the same initial state with respect to the inter-qubit distance  $r_{12}$ . It is clearly seen that the buildup of entanglement is greater for the collective dynamics when compared to the independent one.

Now we take up the issue of entanglement from the perspective of the PDF as in Eq. (3). In figures (4 (a)) and (b), we plot the weights  $\omega_1, \omega_2, \omega_3$  and  $\omega_4$  (3) of the entanglement densities of the projection operators of the various subspaces which span the two qubit Hilbert space with respect to the evolution time  $t$  for the independent and collective decoherence models, respectively, for the case of an interaction with an unsqueezed vacuum bath. Since



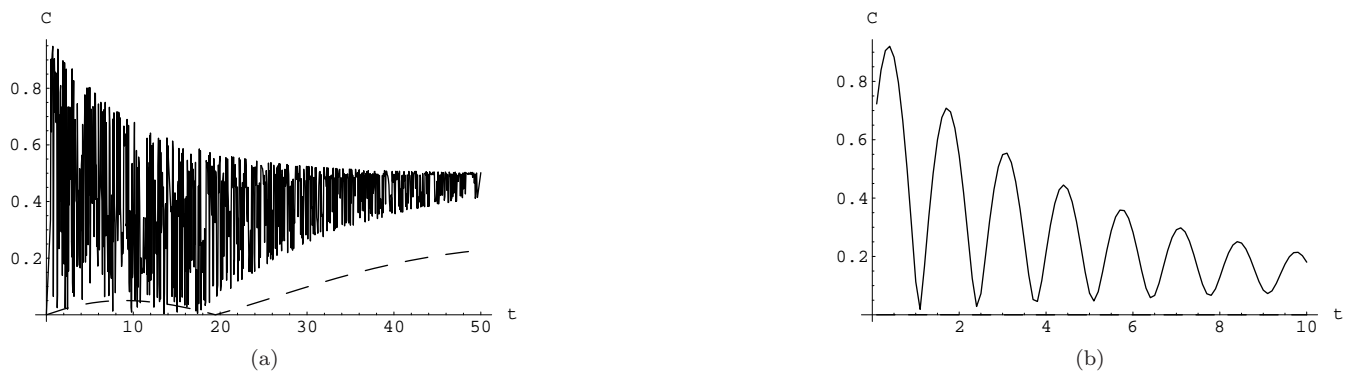


FIG. 2: Concurrence  $\mathcal{C}$  (41) as a function of time of evolution  $t$ . Figure (a) deals with the case of vacuum bath ( $T = r = 0$ ), while figure (b) considers concurrence in the two-qubit system interacting with a squeezed thermal bath, for a temperature  $T = 1$  and bath squeezing parameter  $r$  (9, 10) equal to 0.1. In both the figures the bold curve depicts the collective decoherence model ( $kr_{12} = 0.05$ ), while the dashed curve represents the independent decoherence model ( $kr_{12} = 1.1$ ). In figure (b) for the given settings, the concurrence for the independent decoherence model is negligible and is thus not seen.

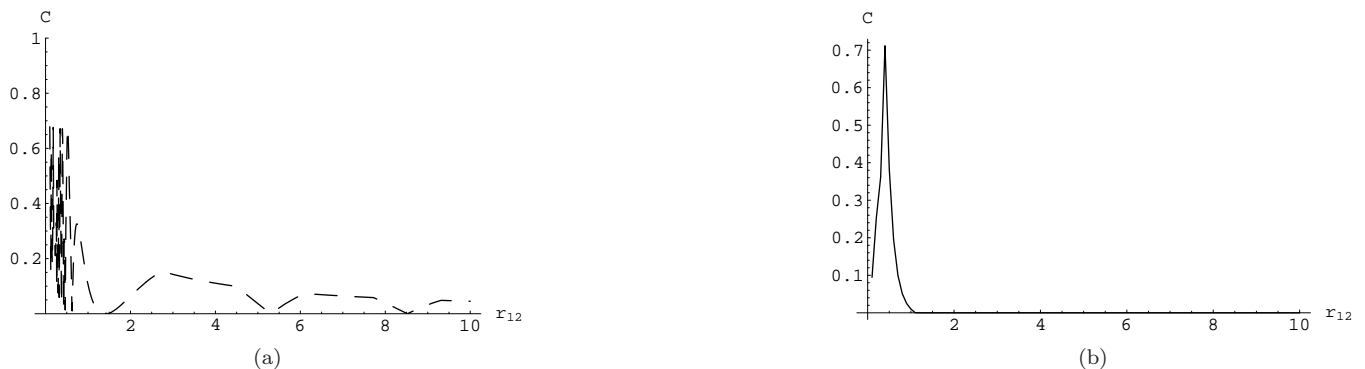


FIG. 3: Concurrence  $\mathcal{C}$  (41) with respect to inter-qubit distance  $r_{12}$ . Figure (a) deals with the case of vacuum bath ( $T = r = 0$ ), while figure (b) considers concurrence in the two-qubit system interacting with a squeezed thermal bath, for  $T = 1$ , evolution time  $t = 1$  and bath squeezing parameter  $r$  (9, 10) equal to 0.1. In figure (a) the oscillatory behavior of concurrence is stronger in the collective decoherence regime, in comparison with the independent decoherence regime ( $kr_{12} \geq 1$ ). In figure (b), the effect of finite bath squeezing and  $T$  has the effect of diminishing the concurrence to a great extent in comparison to the vacuum bath case. Here the concurrence for the independent decoherence regime is negligible, in agreement with the previous figure.

$\omega_1$  is the weight of the one dimensional projection, representing a pure state, and  $\omega_4$  that of the maximally mixed state with  $\omega_2$  and  $\omega_3$  being intermediary, these plots depict the variation in the contribution of the various subspaces to the entanglement of the two-qubit system as  $t$  increases. From the figures it can be seen that in the case of the independent decoherence model, as depicted in figure (4 (a)), the weight  $\omega_2$  dominates the other weights and remains almost constant, while the remaining weights are much lower and their increase is very small compared to it. This is in contrast to the collective decoherence model, wherein we find the weight  $\omega_1$  decreases while  $\omega_2$  increases with time. Since the weight  $\omega_1$  is indicative of pure state entanglement, it is evident from the figures that the entanglement content in the collective decoherence model is higher than that in the independent decoherence model. Also since the weight  $\omega_2$ , representing the weight of the two-dimensional projection operator corresponding to the PDF  $\mathcal{P}_2(\mathcal{E})$ , has a rich entanglement structure, we come to the conclusion that for the case of the two-qubit interaction with a vacuum bath, the entanglement is preserved in the system for a long time. In both the figures, the weight  $\omega_4$ , indicative of a completely mixed state, is negligible over the time range considered.

In figures (5 (a)) and (b), we plot the weights  $\omega_1$ ,  $\omega_2$ ,  $\omega_3$  and  $\omega_4$  (3) of the entanglement densities of the projection operators of the various subspaces which span the two qubit Hilbert space with respect to  $T$  for the independent and collective decoherence models, respectively. These plots thus depict the variation in the contribution of the various subspaces to the entanglement of the two qubit system as  $T$  increases. From figure (5 (b)), we can see that in the collective decoherence regime, the weight  $\omega_1$  initially falls and then stabilizes around a finite value while  $\omega_4$  rises, but remains well below the value of  $\omega_1$ , indicating that for the collective decoherence model, under the given settings, the

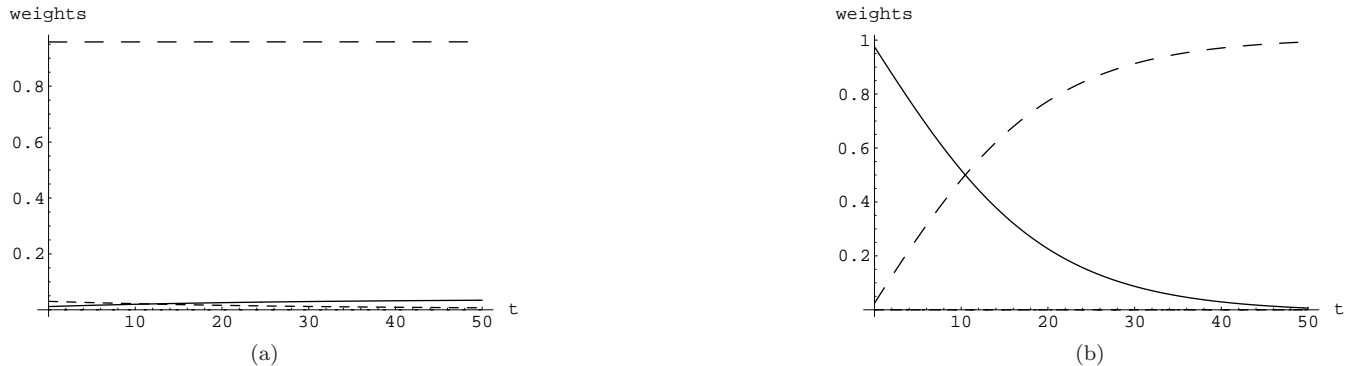


FIG. 4: The weights (3) as a function of evolution time  $t$ , for the case of an interaction with an unsqueezed vacuum bath. Figure (a) refers to the independent decoherence model, with  $kr_{12} = 1.5$  and (b) the collective decoherence model, with  $kr_{12} = 0.08$ . In both the figures, the bold curve corresponds to the weight  $\omega_1$ , while the large-dashed, small-dashed and dotted curves correspond to the weights  $\omega_2$ ,  $\omega_3$  and  $\omega_4$ , respectively. In both the figures, the weight  $\omega_4$  is negligible and hence is not seen.

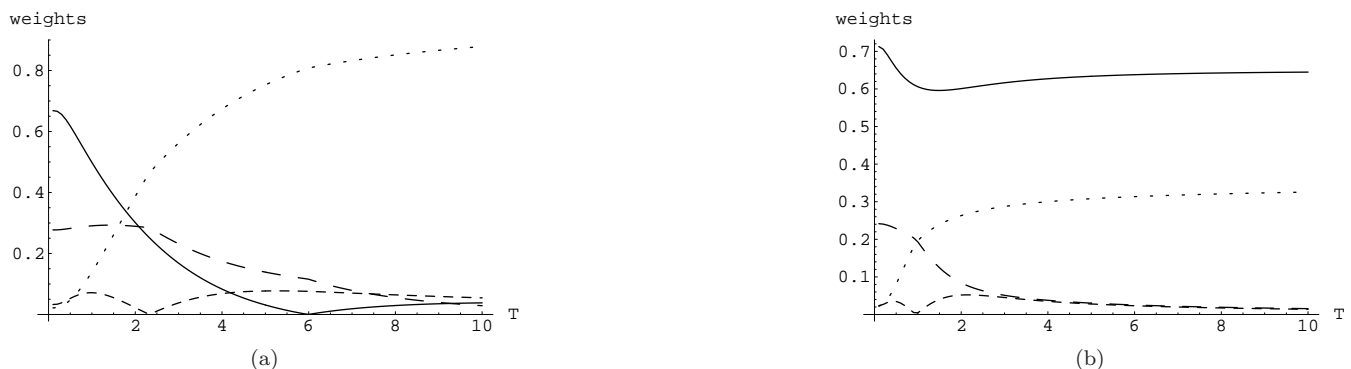


FIG. 5: The weights (3) as a function of temperature  $T$ , for the case of an interaction with a squeezed thermal bath for an evolution time  $t = 5$  and bath squeezing parameter  $r$  (9, 10) equal to 0.5. Figure (a) refers to the independent decoherence model, with  $kr_{12} = 1.5$  and (b) the collective decoherence model, with  $kr_{12} = 0.08$ . In both the figures, the bold curve corresponds to the weight  $\omega_1$ , while the large-dashed, small-dashed and dotted curves correspond to the weights  $\omega_2$ ,  $\omega_3$  and  $\omega_4$ , respectively.

system maintains a finite value of entanglement. This feature is not observed in the figure (5 (a)), where for the same settings,  $\omega_1$  decreases to zero, while  $\omega_4$  rises, thereby indicating a loss of purity and destruction of entanglement.

As explained in Section II, the characterization of MSE for a two-qubit system involves the density function of four projection operators,  $\Pi_1$ ,  $\Pi_2$ ,  $\Pi_3$ ,  $\Pi_4$ , corresponding to one, two, three, and four dimensional projections, respectively. These will be represented here as  $\mathcal{P}_1(\mathcal{E})$ ,  $\mathcal{P}_2(\mathcal{E})$ ,  $\mathcal{P}_3(\mathcal{E})$  and  $\mathcal{P}_4(\mathcal{E})$ , respectively. As also discussed above,  $\mathcal{P}_4(\mathcal{E})$  would be universal for the two-qubit density matrices and would involve the Harr measure on  $SU(4)$  [38]. This is depicted in figure (6) and is common to all the two-qubit PDF of entanglement.

Now we consider the  $\mathcal{P}_2(\mathcal{E})$  and  $\mathcal{P}_3(\mathcal{E})$  density functions for some representative states of the two qubit system, both for the independent as well as collective decoherence models. This enables us to compare the entanglement in the respective subspaces of the system Hilbert space. We also plot the full entanglement density function curve  $\mathcal{P}(\mathcal{E})$  with respect to the entanglement  $\mathcal{E}$ , at a particular time  $t$ . This will enable us to look at the contribution to the entanglement from the different projections.

Figures (7 (a)) and (b) depict the behavior of the density function  $\mathcal{P}_2(\mathcal{E})$  for the bath evolution time  $t = 5.0$  and  $T = 0$  for the independent and collective decoherence models, respectively. For these conditions, the value of concurrence (41) is 0.17 for the case of the independent decoherence model and 0.42 for the collective model, depicting the greater entanglement content in the later compared to the former. This is also borne out by these figures. As shown in [31], the concurrence for a two dimensional projection is  $\mathcal{C}_{\Pi_2} = (\mathcal{E}_{max} - \mathcal{E}_{cusp})/2$ . From the figures (7), it can be seen that the value of  $\mathcal{C}_{\Pi_2}$  is greater for the case of figure (7(b)) when compared to that of figure (7(a)). In all the figures related to the probability density functions of entanglement for the two-qubit system interacting with an unsqueezed vacuum bath, for the independent decoherence model,  $kr_{12}$  is set equal to 1.5, while for the collective decoherence

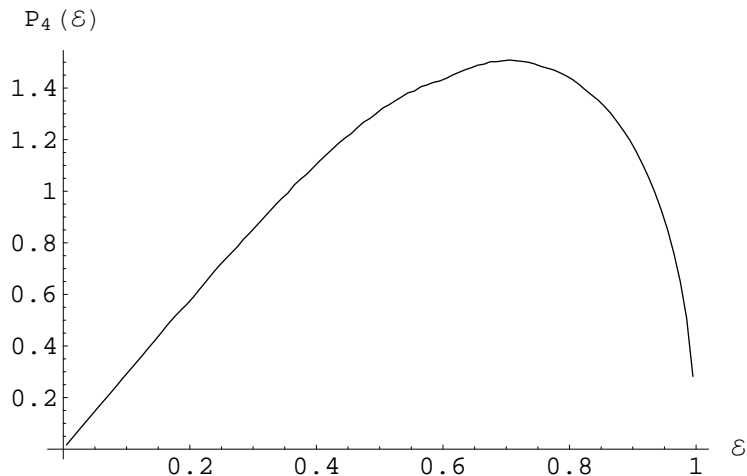


FIG. 6: The PDF for the four dimensional projection spanning the full Hilbert space  $\mathcal{H}(\Pi_4)$ .

model,  $kr_{12}$  is set equal to 0.07. For the two-qubit interaction with a squeezed thermal bath, the independent decoherence model is parametrized as above, while for the collective decoherence model,  $kr_{12}$  is set equal to 0.08. Figures (8 (a)) and (b) exhibit the entanglement density function  $\mathcal{P}_3(\mathcal{E})$  while the figures (9 (a)) and (b) illustrate the behavior of the full density function  $\mathcal{P}(\mathcal{E})$  for the independent and collective decoherence models, respectively and for the same parameters as above. The full entanglement density function is obtained by a weighted sum over all the contributions of the projection operators from the different subspaces (3). Here and in all the subsequent figures for the full PDF, the contribution from the one dimensional projection  $\Pi_1$ , which is a delta function, is represented by a line of height equal to its weight (3) and the point on the abscissa is determined by its corresponding entanglement. The figures (9 (a)) and (b) depict the rich entanglement structure present in the two-qubit system interacting with an unsqueezed vacuum bath. While the contribution in the figure (9 (a)), for the independent decoherence model, comes primarily from the two dimensional projection, that for the collective decoherence model, as in figure (9 (b)), comes from the one and two dimensional projections with the one dimensional projection being the dominant contributor. Since the one dimensional projection represents the pure state entanglement extant in the system, this clearly shows the greater entanglement content in the collective decoherence regime as compared to the independent one. The figures (10 (a)) and (b) show the behavior of the full density function  $\mathcal{P}(\mathcal{E})$  for the independent and collective decoherence models, respectively, for the bath evolution time  $t = 20.0$  and  $T = 0$ . For these parameters, the value of concurrence (41) is 0.32 for the case of the independent decoherence model and 0.54 for the collective model, depicting the greater entanglement content in the later compared to the former. By a comparison with the earlier case for an evolution time  $t = 5$ , is brought out the point that with time there is a build up of entanglement in the two-qubit system. The system is still possessed of a rich entanglement structure. For the independent decoherence model, the principal contribution still comes from the two dimensional contribution but in the collective decoherence regime, in contrast to the earlier case, the principal contribution has now shifted from the one to the two dimensional projection, thereby showing that the system gets more mixed with the passage of time.

We now consider the nature of entanglement in the two-qubit system when it interacts with a squeezed thermal bath. Figures (11 (a)) and (b) depict the behavior of the entanglement density function  $\mathcal{P}_2(\mathcal{E})$  for the evolution time  $t = 1$ ,  $T = 10$  and bath squeezing parameter (9, 10)  $r = 0.5$  for the independent and collective decoherence models, respectively. For these conditions, the value of concurrence (41) is 0, indicating a complete depletion of entanglement. This is partially borne out by the fact that for this case  $\mathcal{C}_{\Pi_2} \approx 0$ . However, as seen from the figures (12 (a)) and (b) and also from the figures (13 (a)) and (b), the system still exhibits a rich entanglement structure. In figure (12 (a)), the parameter  $\mathcal{E}_\perp$  is  $\approx 0.48$  while it is  $\approx 0.98$  for the collective model as in (12 (b)). Since  $\mathcal{E}_\perp$  is evaluated from the state perpendicular to the third non-separable basis in the canonical basis of a three dimensional projection [31], this clearly brings out the greater entanglement content in the collective model as compared to the independent case. In figure (13 (a)), the contribution to the full entanglement density for the independent model comes from the one, two and four dimensional projections with an approximately equal contribution from the one and four dimensional projections while in figure (13 (b)), the contribution to the full entanglement density for the collective model comes from the one and four dimensional projections with the contribution from the one dimensional projection being the dominant one. Since the contribution from the one dimensional projection is an indicator of pure state entanglement in the system, this clearly brings out the entanglement content in the system, under the given conditions, even though concurrence is zero. Also the greater weight carried by the one dimensional projection in the collective model in

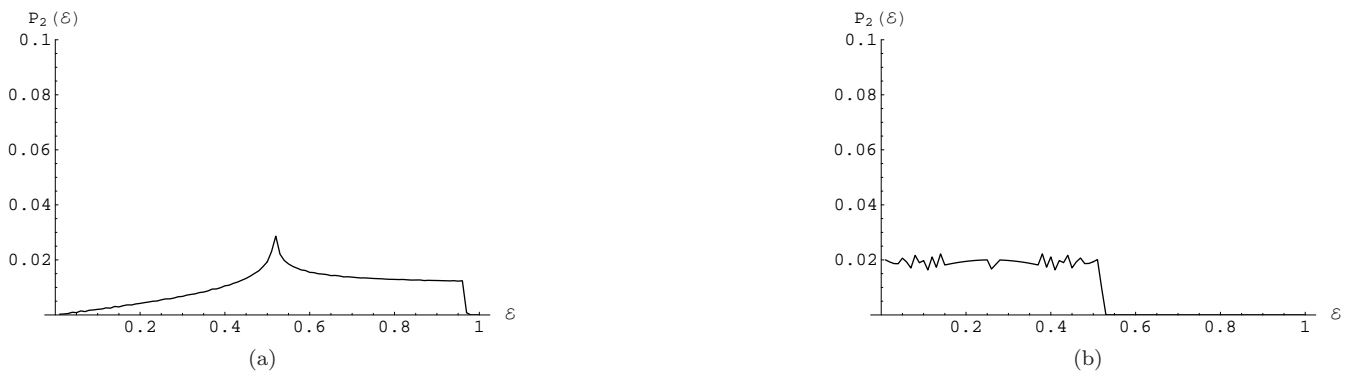


FIG. 7: The density function  $\mathcal{P}_2(\mathcal{E})$  with respect to the entanglement  $\mathcal{E}$  for an evolution time  $t = 5.0$ ,  $T = 0.0$  and bath squeezing parameter  $r$  equal to 0. Figure (a) refers to the independent decoherence model and (b) to the collective decoherence model.

comparison with the independent one, brings out the greater entanglement content in the former.

Figures (14 (a)) and (b) illustrate the full entanglement density for the evolution time  $t = 1$ ,  $T = 10$  and bath squeezing parameter (9, 10)  $r = 1.0$  for the independent and collective decoherence models, respectively. For these conditions, the value of concurrence (41) is zero. However, the system still exhibits an entanglement structure, especially in the collective decoherence regime as seen in the figure (14 (b)) where the one, three and four dimensional projections contribute with the principal contribution coming from the one dimensional projection, thereby indicating the presence of pure state entanglement in the system. The corresponding case for the independent model, as in figure (14 (a)), has its principal contribution coming from the four dimensional projection representing a maximally mixed state. This clearly shows the richer entanglement content in the collective model in comparison to the independent one. Figures (15 (a)) and (b) illustrate the full entanglement density, for the same conditions as above but with zero bath squeezing, for the independent and collective decoherence models, respectively. The entanglement in the system is seen to be greater for this case when compared to the previous cases with finite bath squeezing. The value of concurrence (41) is zero for the independent model, while it is 0.17 for the collective one, bringing out the greater entanglement content in the later in comparison with the former. This is also borne out by the entanglement density function, where the contribution to the full density function from the one dimensional projection (indicative of pure state entanglement) is greater in the collective model when compared to the independent one. Also, in this case of interaction with an unsqueezed thermal bath, the full entanglement density function for the independent decoherence model exhibits greater entanglement when compared to the corresponding case of interaction with a squeezed thermal bath. This seems to indicate that for the two-qubit system, a finite bath squeezing is detrimental to the development of entanglement. Finally in figures (16 (a)) and (b) is depicted the full entanglement density for the evolution time  $t = 5$ ,  $T = 10$  and bath squeezing parameter (9, 10)  $r = 0.5$  for the independent and collective decoherence models, respectively. As expected, with the increase in the exposure to the environment, indicated by the greater evolution time, the system becomes more mixed and hence loses entanglement. This is borne out by the fact that for these conditions, the value of concurrence (41) is zero. However, for the collective decoherence model, as shown in figure (16 (b)), the full density function has contributions coming from the one and four dimensional projections, with the weight carried by the one dimensional projection greater than that by the four dimensional one bringing out the fact that pure state entanglement is still extant in the system under the given conditions. However, for the independent decoherence model, as in figure (16 (a)), the principal contribution to the full entanglement density function comes from the four dimensional projection, indicating that the system is tending towards a maximally mixed state, thereby losing its entanglement.

Thus we see that when compared to the interaction with a bath at  $T = 0$ , the finite  $T$  bath is detrimental to the generation of entanglement between the two-qubit system. An interesting connection of this can be made with the work presented in [39], where the authors connected frustration with interaction strength and ground-state entanglement. They defined frustration as the non-commutativity of the local Hamiltonian (consisting of the single body terms) with the interaction Hamiltonian and argued that with the increase in interaction, ground-state entanglement in the system would increase. The case of dissipative  $S - R$  interaction with  $[H_S, H_{SR}] \neq 0$  would suggest a frustrated system in this nomenclature. For the interaction of the two-qubit system with a vacuum bath, entanglement is seen to rise with increase in the influence of the environment qualitatively agreeing with the above work. Finally entanglement would vanish because as a result of decoherence, the system would lose its quantum coherence and tend towards the classical regime.

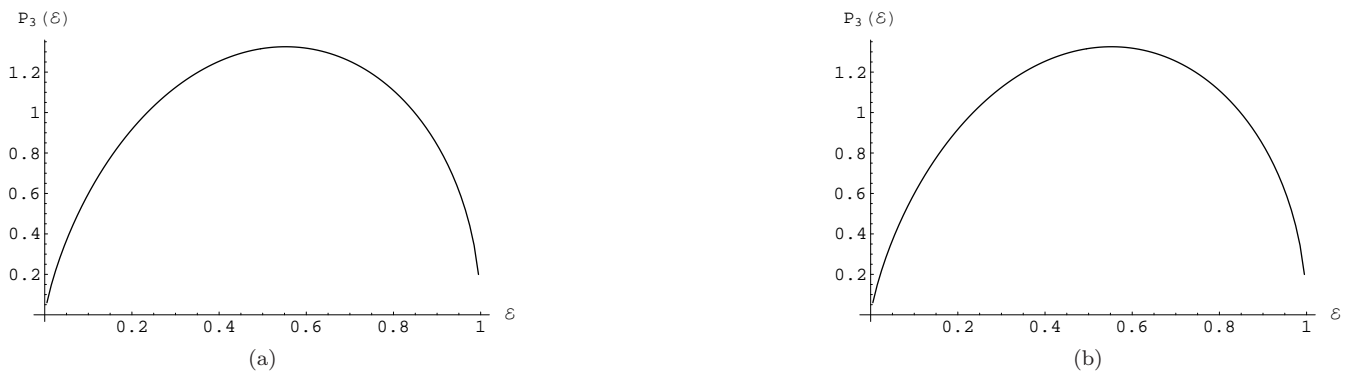


FIG. 8: The density function  $\mathcal{P}_3(\mathcal{E})$  with respect to the entanglement  $\mathcal{E}$  for an evolution time  $t = 5.0$ , and zero  $T$  and bath squeezing. Figure (a) refers to the independent decoherence model and (b) to the collective decoherence model.

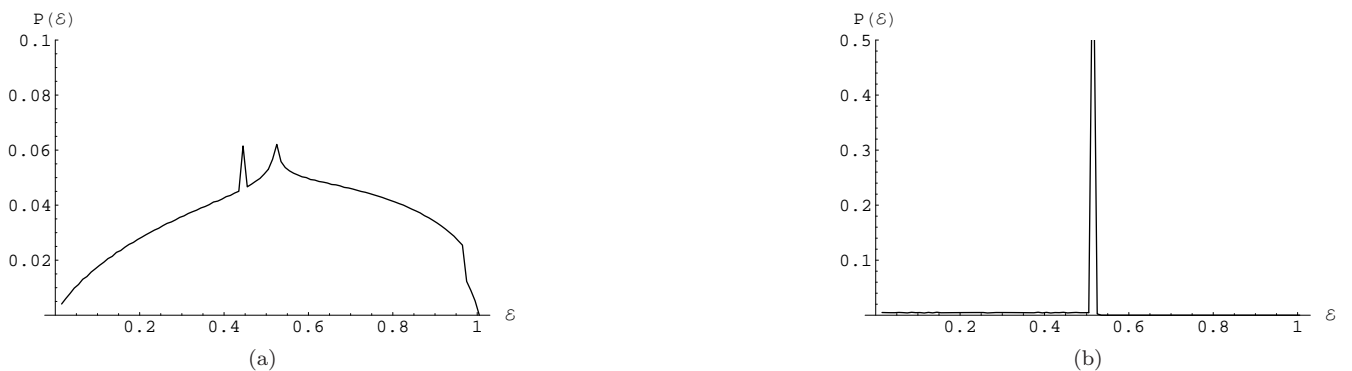


FIG. 9: The full density function  $\mathcal{P}(\mathcal{E})$  (3) with respect to the entanglement  $\mathcal{E}$  for an evolution time  $t = 5.0$ , and zero  $T$  and bath squeezing. Figure (a) refers to the independent decoherence model and (b) to the collective decoherence model.

## VI. AN APPLICATION TO QUANTUM COMMUNICATION: QUANTUM REPEATERS

The technique of entanglement purification [32] can be adapted for quantum communication over long distances, the key idea behind a *quantum repeater* [33]. The efficiency of quantum communication over long distances is reduced due to the effect of noise, which can be considered as a natural open system effect. For distances much longer than the coherence length of a noisy quantum channel, the fidelity of transmission is usually so low that standard purification methods are not applicable. In a quantum repeater set-up, the channel is divided into shorter segments that are

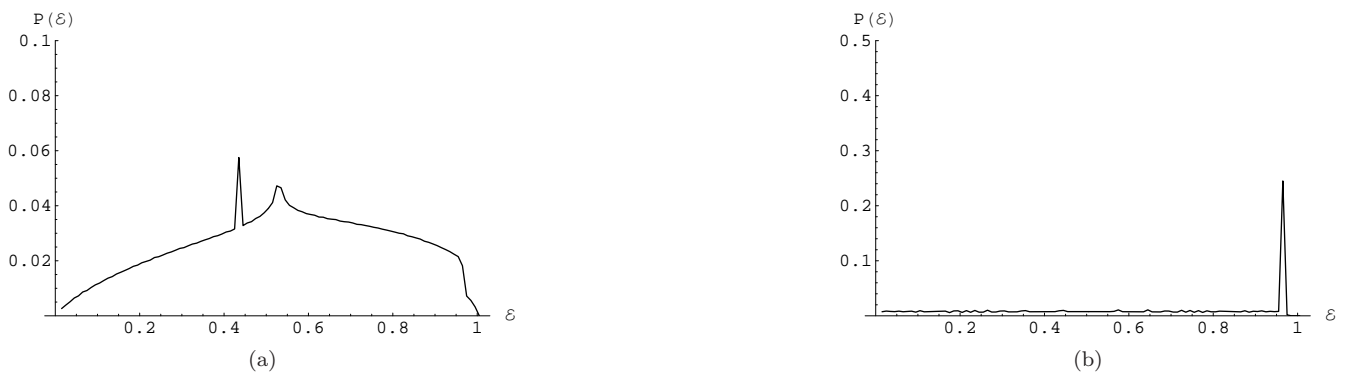


FIG. 10: The full density function  $\mathcal{P}(\mathcal{E})$  (3) with respect to the entanglement  $\mathcal{E}$  for an evolution time  $t = 20.0$ , and zero  $T$  and bath squeezing. Figure (a) refers to the independent decoherence model and (b) to the collective decoherence model.

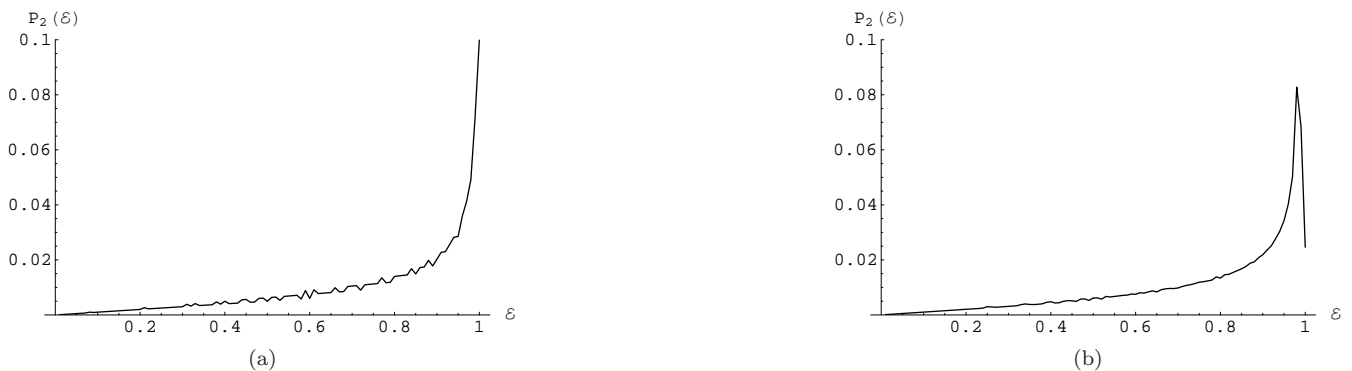


FIG. 11: The density function  $\mathcal{P}_2(\mathcal{E})$  with respect to the entanglement  $\mathcal{E}$  for an evolution time  $t = 1.0$ ,  $T = 10.0$  and bath squeezing parameter  $r$  equal to 0.5. Figure (a) refers to the independent decoherence model and (b) to the collective decoherence model.

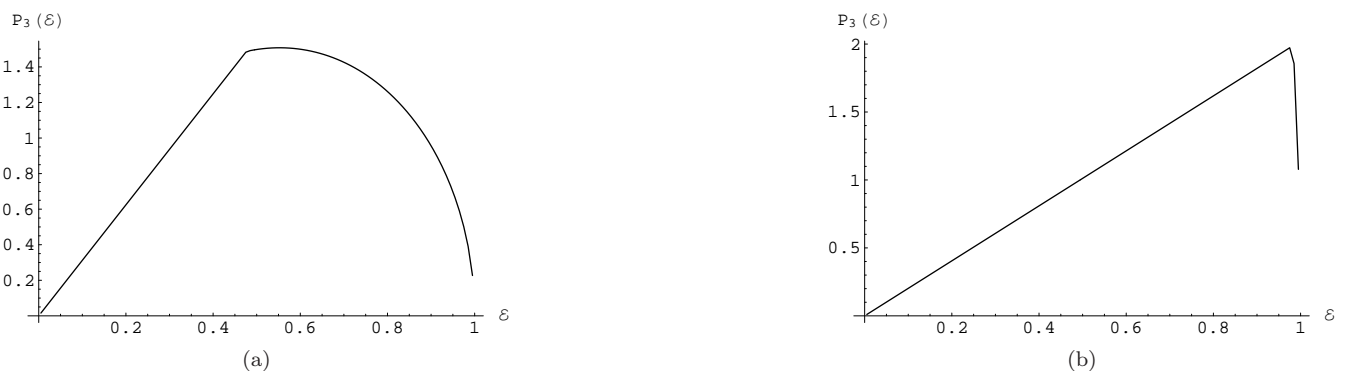


FIG. 12: The density function  $\mathcal{P}_3(\mathcal{E})$  with respect to the entanglement  $\mathcal{E}$  for an evolution time  $t = 1.0$ ,  $T = 10.0$  and bath squeezing parameter  $r$  equal to 0.5. Figure (a) refers to the independent decoherence model and (b) to the collective decoherence model.

purified separately and then connected by the method of entanglement swapping. This method can be much more efficient than schemes based on quantum error correction, as it makes explicit use of two-way classical communication. The quantum repeater system allows entanglement purification over arbitrary long channels and tolerates errors on the percent level. It requires a polynomial overhead in time, and an overhead in local resources that grows only logarithmically with the length of the channel.

We consider the effect of noise, introduced by imperfect local operations that constitute the protocols of entanglement swapping and purification, on such a compound channel, and how it can be kept below a certain threshold. The noise process studied is the one obtained from the two-qubit reduced dynamics via a dissipative system-reservoir interaction, studied above, instead of the depolarizing noise considered in [33]. Here we treat this problem in a simplified fashion, and study the applicability and efficiency of entanglement purification protocols in the situation of imperfect local operations. A treatment of partial teleportation of entanglement, conceptually equivalent to quantum entanglement swapping, in a noisy environment was made in [40].

A quantum repeater involves the two tasks of entanglement swapping, involving Bell-state measurements, and entanglement purification, involving CNOT gates. The Bell-state measurement may be equivalently replaced by a CNOT followed by a projective single-qubit measurement. In entanglement swapping, two distant parties initially not sharing entanglement with each other, but sharing entanglement separately with a third party, become entangled by virtue of a multi-partite measurement by the third party on the latter's two halves of entanglement. Entanglement purification involves two parties employing local operations and classical communication (LOCC) to improve the fidelity  $F$  of Einstein-Podolsky-Rosen (EPR) pairs they share, with respect to a maximally entangled state. The local operations involve two-qubit gates such as the CNOT operation, followed by single qubit measurement, and a possible discarding of an EPR pair. Provided  $F > 0.5$ , and at the cost of losing shared (impure) entanglement, the two parties

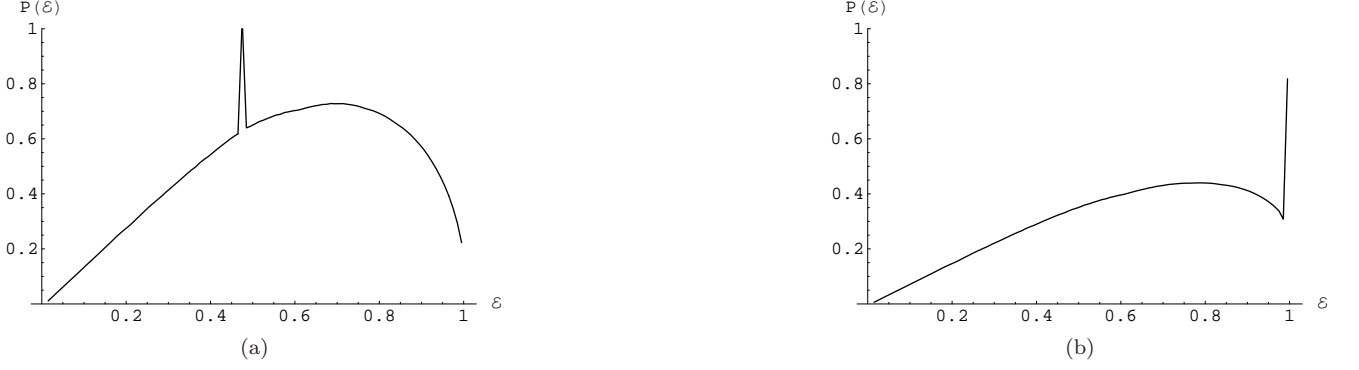


FIG. 13: The full density function  $\mathcal{P}(\mathcal{E})$  (3) with respect to the entanglement  $\mathcal{E}$  for an evolution time  $t = 1$ ,  $T = 10.0$  and bath squeezing parameter  $r$  equal to 0.5. Figure (a) refers to the independent decoherence model and (b) to the collective decoherence model.

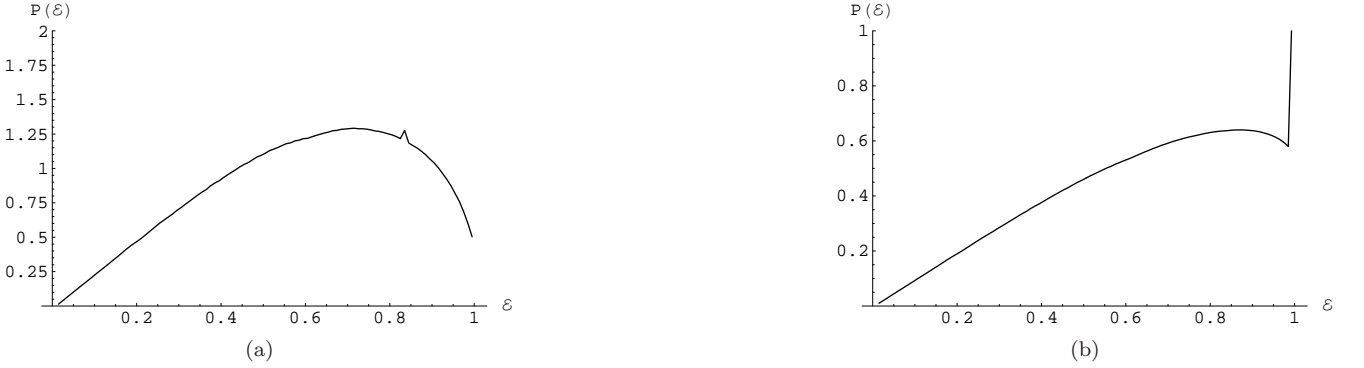


FIG. 14: The full density function  $\mathcal{P}(\mathcal{E})$  (3) with respect to the entanglement  $\mathcal{E}$  for an evolution time  $t = 1$ ,  $T = 10.0$  and bath squeezing parameter  $r$  equal to 1.0. Figure (a) refers to the independent decoherence model and (b) to the collective decoherence model.

can increase the fidelity of the remaining shared entanglement to

$$F' = \frac{F^2 + [(1 - F)/3]^2}{F^2 + [2F(1 - F)/3] + (5/9)(1 - F)^2}, \quad (43)$$

where  $F$  and  $F'$  are, respectively, the input and output fidelities of the entanglement purification protocol proposed by Bennett *et al.* [32].

In the simplified scenario considered here, the output of the noisy CNOT is taken to be a mixed separable state, in place of a pure separable state that is obtained in the noiseless case. As a further simplification, in order to facilitate an easy connection with the purification protocol due to Bennett *et al.*, this mixed state is assumed to be of the form:

$$\rho(F) = F^2 |\uparrow, \downarrow\rangle\langle\uparrow, \downarrow| + (1 - F^2) |\downarrow, \uparrow\rangle\langle\downarrow, \uparrow|, \quad (44)$$

where  $|\uparrow\rangle$  ( $|\downarrow\rangle$ )  $\equiv$   $|\frac{1}{2}\rangle$  ( $|\frac{1}{2}\rangle$ ). Thus,  $\rho(F)$  is a mixture in the two dimensional space spanned by  $\{|\uparrow, \downarrow\rangle, |\downarrow, \uparrow\rangle\}$ , parametrized by fidelity  $F$ , given by  $\sqrt{\langle\uparrow, \downarrow|\rho(F)|\uparrow, \downarrow\rangle}$ . The state  $\rho(F)$  is then the input to the purification protocol, whereby we obtain the output fidelity  $F'$  as a function of  $F$ .

We depict in figures (17 (a)) and (b) the modified ‘purification loop’, obtained by subjecting the noiseless loop to the above model of noise for the independent and collective decoherence regimes, respectively. In both figures we find that noise degrades the performance of the purification protocol. To evaluate its performance, it may be compared with the noiseless case, given by the dot-dashed curve in both figures. That this curve lies above the  $F = F'$  line in the closed range  $[0.5, 1]$  implies that fidelities above the minimum value  $F_{\min} = 0.5$  can be corrected to the maximum value  $F_{\max} = 1$  by repeated application of purification. The degrading effect of noise can be seen in two ways: it introduces an off-set, whereby an input of  $F = 1$  does not yield the same output; it restricts  $F_{\max}$  to values less than 1.





FIG. 15: The full density function  $\mathcal{P}(\mathcal{E})$  (3) with respect to the entanglement  $\mathcal{E}$  for an evolution time  $t = 1$ ,  $T = 10.0$  and bath squeezing parameter  $r$  equal to 0, i.e, we consider here an unsqueezed thermal bath. Figure (a) refers to the independent decoherence model and (b) to the collective decoherence model.

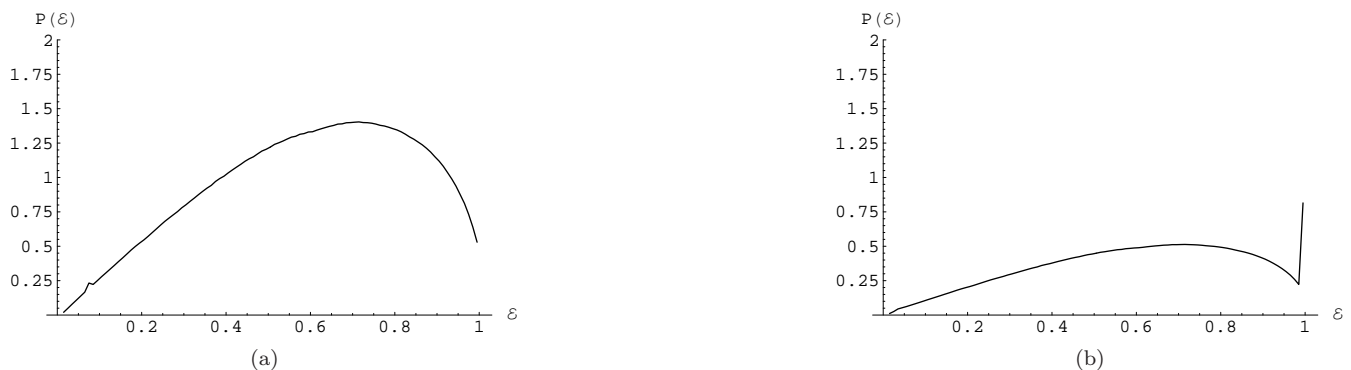


FIG. 16: The full density function  $\mathcal{P}(\mathcal{E})$  (3) with respect to the entanglement  $\mathcal{E}$  for an evolution time  $t = 5$ ,  $T = 10.0$  and bath squeezing parameter  $r$  equal to 0.5. Figure (a) refers to the independent decoherence model and (b) to the collective decoherence model.

In figure (17 (a)), comparison of the small and large dashed curves shows that increasing bath exposure time degrades the fidelity by suppressing  $F_{\max}$  (the point where a curve cuts the  $F = F'$  line from above) and increasing the off-set at  $F = 1$ . Although figure (17 (b)) similarly shows the expected off-set due to noise, the surprising feature is that the curves for  $t = 3$  and  $t = 20$  show a slight *lowering* of output fidelity with increasing input fidelity. The matter is compounded by noting that at an intermediate time ( $t = 14$ ), as depicted by the large-dash-dot curve, the function  $F'(F)$  is monotonously *increasing*. This may be attributed to the fact that entanglement generated due to interaction with the bath shows a strong oscillatory behavior, as seen from figure (2) for the collective regime.

## VII. CONCLUSIONS

Here we have analyzed the dynamics of entanglement in a two-qubit system interacting with its environment, taken to be in a general squeezed thermal state, via a dissipative  $S - R$  interaction. The analysis of the mixed state entanglement has been made using a measure involving a probability density function (PDF).

The position dependent coupling of the qubits with the bath enabled a natural division of the dynamics into an independent and collective decoherence regime, where in the independent decoherence regime the qubits interact via localized  $S - R$  interactions, while in the collective regime the qubits are close enough to feel the bath collectively. The reduced dynamics revealed that in this case of dissipative  $S - R$  interaction, there is no decoherence-free subspace in contrast to that of a QND  $S - R$  interaction [25]. This can be understood in the following manner. As shown in [25], the two-qubit QND reduced dynamics obeys the relation  $\rho_{ab}(t) = \mathcal{L}_{ab}(t)\rho_{ab}(0)$ , with the non-trivial aspect of the dynamics being that  $\mathcal{L}$  represents, not a matrix, but a two-dimensional array, with the multiplication done element-wise. This gets translated into the spin-flip symmetry obeyed by the reduced dynamics. The emergence of a decoherence-free subspace could be attributed to the non-trivial symmetry obeyed by the system. An absence of a

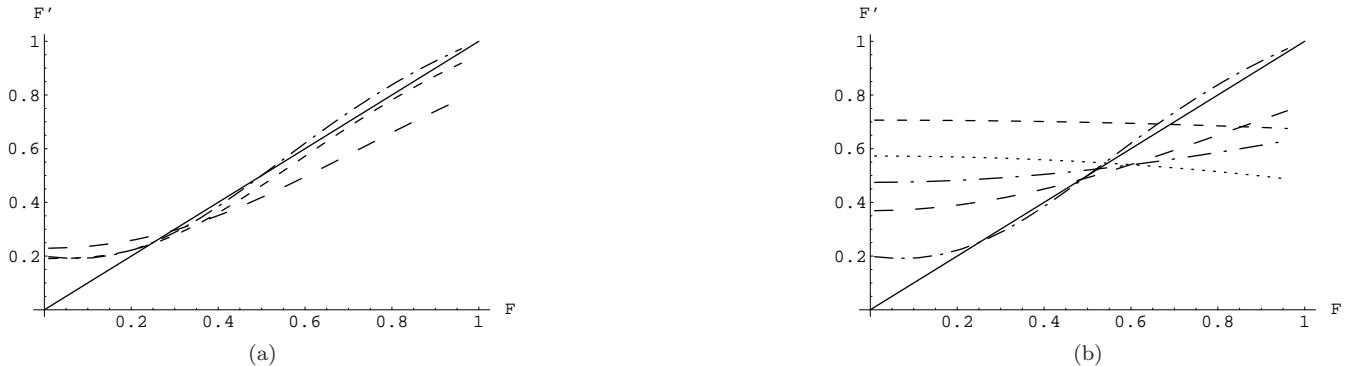


FIG. 17: Purification loop for connecting and purifying EPR pairs. The noisy channel is modelled as a two-qubit dissipative interaction with an unsqueezed vacuum bath in the independent ( $kr_{ab} \geq 1$ ) (plot (a)) and collective ( $kr_{ab} \ll 1$ ) (plot (b)) decoherence regime, with the input state given by  $\rho(F)$  in Eq. (44). The bold line is the  $F = F'$  plot, the small and large dashed curves represent  $t = 3$  and  $t = 10$ , respectively, while the dot-dashed curve is due to the noiseless Bennett et al. protocol. In (b), the larger dash-dot curve and the dotted curves represent, respectively,  $t = 14$  and  $t = 20$ , respectively.

decoherence-free subspace in the present case of dissipative interaction could be due to the lack of such a symmetry in the reduced dynamics.

We studied the entanglement in the two-qubit system for different bath parameters, for both vacuum as well as a bath at finite  $T$  and squeezing and used the measure of mixed state entanglement involving a PDF as well as concurrence. It clearly emerged that entanglement generation is more efficient in the case of interaction with a bath at zero  $T$  than at finite  $T$ . It also appears that in this case of two-qubit dissipative  $S - R$  interaction, presence of finite bath squeezing does not help in entanglement generation. This is in contrast to expectations from the single-qubit dissipative interaction [36] where it was observed that for some bath parameters, the process of decoherence could be slowed down resulting in the preservation of quantum coherence for a longer time. It would be pertinent to point out here an interesting work [41] where the authors studied in detail the evolution of entanglement between two oscillators coupled to the same environment. There the oscillator system was assumed to start from a general two-mode Gaussian state, which includes the two-mode squeezed state. Entanglement in the final state was considered as a resource whose origin could be the quantum resource available in the system, viz. squeezing in the initial oscillator system. It was shown that under certain regimes of the squeezing parameter, the environment could be used as a resource to extract entanglement, thereby highlighting the importance of squeezing in the study of entanglement generation. The work presented here differs from that in [41], apart from the obvious difference in the system (here a two-qubit system), in that the evolution considered here is Markovian while that in [41] is that of quantum Brownian motion which is essentially non-Markovian. Also, here the squeezing originated from the bath while that in [41] was in the initial system state. It would be of interest to extend the work presented here to have a better understanding of the impact of squeezing, a natural resource, on the dynamic evolution of entanglement.

The entanglement analysis via the PDF showed an advantage over concurrence, specially in the case of mixed state entanglement due to interaction with a finite  $T$  bath. While concurrence was zero for most of the cases considered, the PDF revealed the structure of entanglement still present in the two-qubit system bringing out the statistical and geometrical nature of the measure. Finally we made an application of the dissipative two-qubit reduced dynamics to a simplified model of a quantum repeater, which can be adapted for quantum communication over long distances. Thus this work along with [25] makes a detailed study of the dynamics of two-qubit entanglement in the presence of generic, purely dephasing as well as dissipative, open quantum system effects.

### Acknowledgments

We wish to thank Shanthanu Bhardwaj for numerical help.

- 
- [1] W. H. Louisell, *Quantum Statistical Properties of Radiation* (John Wiley and Sons, 1973).  
 [2] A. O. Caldeira and A. J. Leggett, *Physica A* **121**, 587 (1983).

- [3] W. H. Zurek, Phys. Today **44**, 36 (1991); Prog. Theor. Phys. **87**, 281 (1993).
- [4] S. Banerjee and R. Ghosh, J. Phys. A: Math. Theo. **40**, 13735 (2007); eprint quant-ph/0703054.
- [5] V. Hakim and V. Ambegaokar, Phys. Rev. A **32**, 423 (1985).
- [6] C. M. Smith and A. O. Caldeira, Phys. Rev. A **36**, 3509 (1987); *ibid* **41**, 3103 (1990).
- [7] H. Grabert, P. Schramm and G. L. Ingold, Phys. Rep. **168**, 115 (1988).
- [8] S. Banerjee and R. Ghosh, Phys. Rev. A **62**, 042105 (2000).
- [9] S. Banerjee and R. Ghosh, Phys. Rev. E **67**, 056120 (2003).
- [10] C. J. Myatt, B. E. King, Q. A. Turchette, C. A. Sackett, *et al.*, Nature **403**, 269 (2000).
- [11] Q. A. Turchette, C. J. Myatt, B. E. King, C. A. Sackett, *et al.*, Phys. Rev. A **62**, 053807 (2000).
- [12] J. S. Bell, Physics **1**, 195 (1964).
- [13] M. Nielsen and I. Chuang, *Quantum Computation and Quantum Information* (Cambridge University Press, Cambridge, 2000).
- [14] P. Shor, SIAM Journal of Computing **26**, 1484 (1997); L. K. Grover, Phys. Rev. Lett. **79**, 325 (1997).
- [15] S. Calderbank and P. Shor, Phys. Rev. A **54**, 1098 (1996); A. Steane, Proc. Roy. Soc., London, Ser. A **452**, 2551 (1996).
- [16] A. Beige, D. Braun, B. Tregenna and P. L. Knight, Phys. Rev. Lett. **85**, 1762 (2000).
- [17] M. Fleischhauer, S. F. Yelin and M. D. Lukin, Opt. Commun. **179**, 395 (2000).
- [18] S. Schneider and G. J. Milburn, Phys. Rev. A **65**, 042107 (2002).
- [19] H.-P. Breuer and F. Petruccione, *The Theory of Open Quantum Systems* (Oxford University Press 2002).
- [20] D. Wilson, J. Lee and M. S. Kim, J. Mod. Optics **50**, 1809 (2003).
- [21] R. Simon, Phys. Rev. Lett. **84**, 2726 (2000).
- [22] L. D. Contreras-Pulido and R. Aguado, Phys. Rev. B **77**, 155420 (2008).
- [23] M. P. Almeida, F. de Melo, M. Hor-Meyll, A. Salles, *et al.*, Science **316**, 579 (2007); A. Salles, F. Melo, M. P. Almeida, M. Hor-Meyll, *et al.*, arXiv:0804.4556.
- [24] J. Laurat, K. S. Choi, H. Deng, C. W. Chou, and H. J. Kimble, Phys. Rev. Lett. **99**, 180504 (2007).
- [25] S. Banerjee, V. Ravishankar and R. Srikanth, eprint arXiv:arXiv:0810.5034.
- [26] R. Srikanth and S. Banerjee, Phys. Rev. A **77**, 012318 (2008); arXiv:0707.0059.
- [27] C. H. Bennett, D. P. DiVincenzo, J. A. Smolin and W. K. Wootters, Phys. Rev. A **54**, 3824 (1996).
- [28] W. K. Wootters, Phys. Rev. Lett. **80**, 2245 (1998).
- [29] F. Mintert, A. R. R. Carvalho, M. Kus and A. Buchleitner, Phys. Reports **415**, 207 (2005).
- [30] R. F. Werner, Phys. Rev. A **40**, 4277 (1989).
- [31] S. Bhardwaj and V. Ravishankar, Phys. Rev. A **77**, 022322 (2008).
- [32] C. H. Bennett, G. Brassard, S. Popescu, B. Schumacher *et al.*, Phys. Rev. Lett. **76**, 722 (1996).
- [33] H.-J. Briegel, W. Dür, J. I. Cirac and P. Zoller, Phys. Rev. Lett. **81**, 5932 (1998); W. Dür, H.-J. Briegel, J. I. Cirac, and P. Zoller, Phys. Rev. A **59**, 169 (1999).
- [34] Z. Ficek and R. Tanaś, Phys. Rep. **372**, 369 (2002).
- [35] S. Banerjee and R. Srikanth, to appear in Eur. Phys. J. D; eprint quant-ph/0611161.
- [36] S. Banerjee and R. Srikanth, Phys. Rev. A **76**, 062109 (2007); eprint: arXiv:0706.3633.
- [37] R. H. Dicke, Phys. Rev. **93**, 99 (1954).
- [38] T. E. Tilma, M. Byrd and E. C. G. Sudarshan, J. Phys. A: Math. Gen. **35**, 9255 (2002).
- [39] C. M. Dawson and M. A. Nielsen, arXiv:quant-ph/0401061.
- [40] J. Lee, M. S. Kim, Y. J. Park and S. Lee, J. Mod. Optics **47**, 2151 (2000).
- [41] J. P. Paz and A. J. Roncaglia, arXiv:0809.1676; Phys. Rev. Lett. **100**, 220401 (2008).